Supplement of Biogeosciences, 23, 3541–3565, 2026
https://doi.org/10.5194/bg-23-3541-2026-supplement

Biogeosciences Open Access EGU

Supplement of

Using different radiative transfer schemes for solar-induced chlorophyll fluorescence (SIF) in evergreen coniferous forests with a terrestrial biosphere model

Tea Thum et al.

Correspondence to: Tea Thum (tea.thum@fmi.fi)

Contents of the supplementary material

S1 Model and metrics description

S1.1 QUINCY: Calculation of leaf chlorophyll from leaf nitrogen

Leaf nitrogen content in QUINCY has a vertical gradient that decreases exponentially towards the bottom of the canopy, in accordance with observations (Niinemets et al., 1998). Leaf N in each layer ($N_{leaf,cl}$) consists of structural and photosynthetic parts (Friend et al., 1997). The photosynthetic N pools are divided into three compartments: Rubisco associated (fN_{rub}), electron transport associated (fN_{et}), and chlorophyll associated (fN_{chl}). In order to calculate the chlorophyll associated compartment, the structural part of leaf N needs to be estimated first.

The fraction of structural N ($fN_{struc,cl}$) is calculated for each canopy layer as a function of the total leaf N in the respective layer (Zaehle and Friend, 2010):

$$fN_{struc,cl} = k_0^{struc} - k_1^{struc} N_{leaf,cl} \tag{S1}$$

where k_0^{struc} is the maximum fraction of structural leaf N (0.83 for coniferous forest (Friend et al., 1997; Kattge et al., 2011)) and k_1^{struc} is the slope of structural leaf N with total N (7.14 $\times 10^3$ $g^{-1}N$) (Friend et al., 1997) .

According to Zaehle and Friend (2010), the fraction of leaf N in chlorophyll is calculated to increase with canopy depth:

$$fN_{chl} = \frac{k_0^{chl} - k_1^{chl} e^{-k_{fn}^{chl} LAI_c}}{a_{chl}^n}, \tag{S2}$$

where k_0^{chl} (value 6.0 (Zaehle and Friend, 2010)), k_1^{chl} (value 3.6 (Zaehle and Friend, 2010)) and k_{fn}^{chl} (value 0.7 (Friend, 2001)) are empirical parameters. a_{chl}^n is the molecular N content of chlorophyll (25.12 $\frac{\text{mol}}{\text{mmol}^{-1}}$ (Evans, 1989)). LAI_c is the cumulative leaf area.

S1.2 QUINCY: Calculation of stomatal conductance

Stomatal conductance for one canopy layer ($g_{s,cl}$) is calculated as (we have removed the subscript cl from the following equation) (Medlyn et al., 2011):

$$g_s = [g_0 + g_1 \frac{A_n \beta_{air} \beta_{soil}^{gs}}{c_a}] \times R \times T_{air}/p \tag{S3}$$

where g_0 and g_1 are PFT-specific constants, A_n is the leaf-level net photosynthesis, R is the molar gas constant, T_{air} is air temperature (K) and p air pressure (Pa).

S1.3 QUINCY: Using state of acclimation in slowing down spring recovery in evergreen forests

The onset of photosynthesis for evergreen coniferous forests is delayed as a function of air temperature in QUINCY (Thum et al., 2019). The use of a constant temperature response for the photosynthesis parameters $J_{max,25}$ and $V_{c(max),25}$ has been shown to predict too early spring recovery in boreal coniferous forests (Thum et al., 2008). Therefore, a more accurate representation of delayed spring onset of these parameters has been adapted from Mäkelä et al. (2019) and parameterized using several sites from the FLUXNET database (Baldocchi et al., 2001). The formulation for the state of acclimation (SOA) (S) is (Mäkelä et al., 2004):

$$\frac{dS}{dt} = \frac{1}{\tau_{soa}}(T_{air} - S) \tag{S4}$$

where τ_{soa} is a time constant (114 hours) and T_{air} is the air temperature. Therefore, S is a delayed temperature sum. It is used to calculate a delay factor (β_{soa}) for photosynthesis (used as a multiplier for the parameters $V_{c(max,25)}$ and $J_{max,25}$ as described in Thum et al. (2019)):

$$\beta_{soa} = \frac{1}{1 + e^{b(S - T_s)}} \tag{S5}$$

where b (°C^{-1}) and T_s (°C) are parameters, set to -0.5 °C^{-1} and 5.0 °C, respectively.

S1.4 Leaf level model of chlorophyll fluorescence

We applied the widely used leaf level model for steady-state leaf chlorophyll fluorescence developed by van der Tol et al. (2014). It is part of the Soil Canopy Observation, Photochemistry and Energy fluxes (SCOPE) model (van der Tol et al., 2009) and its derivatives, such as mSCOPE (Yang et al., 2017). Here, we briefly introduce the equations of this leaf model to clarify

its implementation in QUINCY. We could not directly follow the implementation in SCOPE, because QUINCY has a different formulation for the photosynthesis model, which is described in section 2.4. For a detailed description of the model leaf level ChlF model, see van der Tol et al. (2014). We have used all the default parameters of the leaf level model and have not adjusted them.

The ChlF pathway of involving excitations in the leaves will be denoted by F, photochemistry by P. Heat dissipation is divided into a constitutive thermal dissipation, denoted by D, and an energy-dependent heat dissipation, denoted by N, and this is NPQ. D is present also in dark-adapted plants, while N is more variable and controlled by the electron transport of the photosystems. Below we introduce the reversible NPQ and in the Section 2.7 also a formulation for the sustained NPQ, which is an additive term to the reversible NPQ.

The relative rate coefficients (K) express the probability of different rates of excitation and can be used to express the yield:

$$\Phi_P = \frac{K_P}{\sum K} \tag{S6a}$$

$$\Phi_F = \frac{K_F}{\sum K} \tag{S6b}$$

$$\Phi_D = \frac{K_D}{\sum K} \tag{S6c}$$

$$\Phi_N = \frac{K_N}{\sum K} \tag{S6d}$$

$$\sum K = K_P + K_F + K_D + K_N \tag{S6e}$$

These rates are mutually exclusive, and therefore the yield of all processes is:

$$\Phi_P + \Phi_F + \Phi_D + \Phi_N = 1 \tag{S7}$$

The rate coefficient K_F is constant and K_D depends on the air temperature (T_{air} in °C) as estimated from measurements by (van der Tol et al., 2014):

$$K_D = MAX(0.8738, 0.0301 \frac{1}{^\circ C} * T_{air} + 0.0773) \tag{S8}$$

while K_N and K_P are influenced by the metabolic state of the leaves.

According to Genty et al. (1989), the Φ_P at the steady state can be calculated from the ratio of the variable fluorescence ($F'_m - F_t$) to the maximum fluorescence in light (F'_m), as

$$\Phi_P = \frac{F'_m - F_t}{F'_m} \tag{S9}$$

where F_t is the steady-state fluorescence. Yields can be expected to follow the Genty relationship:

$$\Phi_{F_t} = (1 - \Phi_P)\Phi_{F'_m} \tag{S10}$$

where Φ_{F_t} is the steady-state fluorescence yield and $\Phi_{F'_m}$ is the yield of maximum fluorescence in light, obtained with a saturating pulse in the PAM observations. To evaluate $\Phi_{F'_m}$, we note that the rate coefficient of photosynthesis K_P goes to zero with the saturating light pulse, since then all the open PSII reaction centers are closed by the pulse. Because of this and Eq. (S6c) we get

$$\Phi_{F'_m} = \frac{K_F}{K_F + K_D + K_N} \tag{S11}$$

and here only K_N is unknown. van der Tol et al. (2014) developed an experimental relationship to relate K_N to the changes in Φ_P. The K_N that controls F'_m must be related to the relative decrease in the photochemical yield. To achieve this, a factor x (degree of the light saturation) is defined which is zero when photochemistry is working at full efficiency and one when photochemistry is completely absent. This is

$$x = 1 - \frac{\Phi_P}{\Phi_P^0} \tag{S12}$$

where Φ_P^0 is the maximum photochemical yield which can be observed under dark adapted and low light conditions.

In the original SCOPE formulation, the constraint imposed on Φ_P is calculated as the fraction of actual electron transport compared to potential electron transport. Since QUINCY has a different formulation for photosynthesis, we calculated the limitation on Φ_P as a fraction of actual electron transport compared to the case where the whole leaf would be light limited, i.e. there would be no light-saturated region at all. In principle, our solution is similar to the standard SCOPE formulation, although the formulation of the photosynthesis model is slightly different.

The steady-state chlorophyll fluorescence yield is

$$\Phi_{F_t} = (1 - \Phi_P^0 + x\Phi_P^0)\Phi_{F'_m} \tag{S13}$$

The empirical relationship based on measurements of cotton leaves between x and K_N is (van der Tol et al., 2014)

$$K_N = \frac{(1+\beta)x^\alpha}{\beta + x^\alpha} K_N^0 \tag{S14}$$

where the parameters are K_N^0 = 2.48, α = 2.83 and β = 0.114. These are for the standard conditions, while the van der Tol et al. (2014) also gives parameter values for water-limited conditions. This is the reversible part of the K_N, which we will refer to as $K_{N_{rev}}$ in the Section 2.7.

The chlorophyll fluorescence yield can be used to calculate the SIF emission from photosystems per leaf layer $\mathrm{SIF_{internal}}$,

$$SIF_{internal} = Sun_{frac} PPFD_{sun} \Phi_{F_t,sun} + (1 - Sun_{frac}) PPFD_{sha} \Phi_{F_t,sha} \tag{S15}$$

where $\mathrm{PPFD_{sun}}$ is the absorbed photosynthetically active radiation (PAR) for the sunlit leaves, $\mathrm{PPFD_{sha}}$ for the shaded leaves and $\mathrm{Sun_{frac}}$ is the fraction of the sunlit leaves. The $\Phi_{F_t,sun}$ is the fluorescence yield calculated for the sunlit leaves and $\Phi_{F_t,sha}$ for the shaded leaves. Sections 2.5.1-2.5.3 describe the different ways in which this emission has been scaled up to the leaf and canopy level. To obtain the emission per layer, it needs to be multiplied by the LAI of that layer.

S1.5 L2SM equations

The L2SM equations are calculated separately for the visible and the near infrared regions. The total solar induced fluorescence SIF_{canopy} leaving a canopy of L layers, is

$$SIF_{canopy} = \sum_{l=1}^{L} \frac{SIF_{layer}}{2} \left[\frac{T_{l-\frac{1}{2}}(1 + R_{L-l-\frac{1}{2}})}{1 - R_{l-\frac{1}{2}} R_{L-l-\frac{1}{2}}} \right], \tag{S16}$$

where $R_{l-\frac{1}{2}}$ is the reflectance of the entire canopy above the middle of layer l and $T_{l-\frac{1}{2}}$ is the transmittance of the same. $R_{L-l-\frac{1}{2}}$ is the reflectance of everything below the middle of layer l, including the soil.

SIF_{layer} is the SIF emission from the layer, and in the formulation used here it is assumed to be equal in the upward and downward directions and to emerge from the middle of the layer. To find the bulk optical properties of the combined layers used in Equation S16 the reflectance and transmittance of individual layers are combined using the technique of adding, so the reflectance (R_+) of two layers is given by

$$R_+ = R_1 + T_1^2 R_2 R_M, \tag{S17}$$

where R_1 is the reflectance due to diffuse radiation from the upper layer, T_1 is the transmittance due to diffuse radiation of the upper layer and R_2 is the reflectance due to diffuse radiation from the lower layer (which could also be the soil). R_M takes into account multiple diffuse reflections between layers and is given by

$$R_M = \frac{1}{1 - R_1 R_2}. \tag{S18}$$

An addition to earlier implementations of L2SM (e.g Knorr et al. (2025)) is that the attenuation of the SIF signal inside the leaf was taken into account. In this approach the leaf was split into two halves with equal optical depth and it was assumed that the SIF emission originated from between those two layers.

Splitting the leaf in half optically is done by inverting the doubling equation, resulting in:

$$\tau_{\frac{1}{2}} = \left(\tau \left(1 - \rho_{\frac{1}{2}}^2\right)\right)^{\frac{1}{2}}, \tag{S19}$$

and:

$$\rho_{\frac{1}{2}} = \frac{\rho}{1 + \tau}. \tag{S20}$$

We use ρ and τ to represent the (whole) leaf reflectance and transmittance respectively (to avoid confusion with the bulk optical properties of the layer, given by R and T), and the sub-scripted $\frac{1}{2}$ to indicate the corresponding optical property for a half leaf. Given values for ρ and τ, and the leaf internal chlorophyll fluorescence ($SIF_{internal}$) at the required wavelength, we can then calculate the leaf leaving SIF:

$$SIF_{leaf} = \frac{\tau_{\frac{1}{2}}}{1 - \rho_{\frac{1}{2}}^2} \, SIF_{internal}. \tag{S21}$$

The value of the leaf-leaving SIF is then scaled to the amount being emitted with the layer by the layer LAI, i.e.:

$$SIF_{layer} = LAI \times SIF_{leaf} \tag{S22}$$

S1.6 Formulas for metric calculations

The formula for r^2 is

$$r^2 = 1 - \frac{\sum_{i=1}^{n} (y_i - \hat{y})^2}{\sum_{i=1}^{n} (y_i - \bar{y})^2} \tag{S23}$$

where y_i is observation, $\bar{y}$ is the mean of observations, $\hat{y}$ is the model prediction and n is the number of observations.

The bias can be calculated as

$$\text{Bias} = \frac{1}{N}\sum_{i=1}^{N}(\hat{y}_i - y_i) \tag{S24}$$

The RMSE is defined as

$$RMSE = \sqrt{\frac{1}{n}\sum_{i=1}^{n}(y_i - \hat{y}_i)^2} \tag{S25}$$

Additionally we used RMSE separated for systematic ($\mathrm{RMSE_{sys}}$) and random error ($\mathrm{RMSE_{ran}}$) (Willmott, 1981). $\mathrm{RMSE_{sys}}$ is:

$$RMSE_{sys} = \sqrt{\frac{1}{n}\sum_{i=1}^{n}(\hat{y}_i^* - \hat{y}_i)^2} \tag{S26}$$

,

where $\hat{y}_i^*$ is regression-estimated prediction and $\mathrm{RMSE_{ran}}$ is

$$RMSE_{ran} = \sqrt{\frac{1}{n}\sum_{i=1}^{n}(y_i - \hat{y}_i^*)^2} \tag{S27}$$

S1.7 Unit conversion

In the unit conversion, the Planck equation is used to obtain the energy E of photons per mole as

$$E = \frac{N_a hc}{\lambda_\phi} \tag{S28}$$

where N_a is Avogadro's number (value is $6.022 \cdot 10^{23}$), h is the Planck's constant ($6.626 \cdot 10^{-34}\ Js$), c is the speed of light ($3.0 \cdot 10^8\ m\,s^{-1}$) and λ_ϕ is the wavelength of the SIF photons (unit m).

The emittance of SIF from the top of the canopy is assumed to be isotropic, so the conversion to steradians is done using a constant factor of $\frac{1}{\pi}$. The final step is to weight the relative strength of the emissions at wavelengths λ_ϕ compared to a reference SIF spectrum as:

$$w = \frac{e_s(\lambda_\phi)}{\sum_i e_s(\lambda_{\phi,i})}, \tag{S29}$$

where e_s is the emission spectrum in relative units. The emission was calculated for the wavelengths of the observing instruments (PhotoSpec or FloX). Similarly to Knorr et al. (2025), we used a spectrum observed at Hyytiälä Scots pine forest, located in central Finland (Magney et al., 2019; Magney and Frankenberg, 2019) for the LZ approach. Observations of four trees were made at a light level of 1200 $\mu\mathrm{mol\,m^{-2}\,s^{-1}}$ and these spectra were then averaged. For the L2SM we used mathematically constructed estimate of the *in vivo* leaf spectrum (Gordon, 1979), which was based on double Gaussian curve and normalized to one. This was done, since the current version of L2SM includes the leaf attenuation of the SIF signal.

Using this information, the unit conversion of the original SIF, $SIF_{unit,flux}$, to the SIF in measured units, $SIF_{unit,eng}$ is obtained as follows:

$$SIF_{unit,eng} = SIF_{unit,flux}\frac{e_{sw}}{\pi}. \tag{S30}$$

S2 Supplementary tables

Table S1. Variables and parameters of leaf level chlorophyll fluorescence model, including values held constant. All the parameter values are from (van der Tol et al., 2014). Acronym "r.u." refers to relative units.

Variable name (unit)	Symbol	Value
Relative rate coefficient for photosynthesis (-)	K_P	-
Relative rate coefficient for fluorescence (-)	K_F	0.05
Relative rate coefficient for constitutive heat dissipation (-)	K_D	Eq. (S8)
Relative rate coefficient for energy-dependent heat dissipation (-)	K_N	-
Yield for photosynthesis (-)	Φ_P	-
Yield for fluorescence (-)	Φ_F	-
Yield for constitutive heat dissipation (-)	Φ_D	-
Yield for energy-dependent heat dissipation (-)	Φ_N	-
Maximum fluorescence in light (r.u.)	F'_m	-
Steady-state fluorescence (r.u.)	F_t	-
Yield of maximum fluorescence in light	$\Phi_{F'_m}$	-
Maximum photochemical yield in dark adapted state	Φ_P^0	-
Maximum photochemical yield in dark adapted state	Φ_P^0	-

Table S2. The r^2 and RMSE values of simulated versus observed red and far-red region SIF values, according to different radiative transfer approaches at US-NR1. The metrics are also shown for GPP, which is from default QUINCY configuration. The morning values are from 6 a.m. to 9:30 a.m., midday values from 10 a.m. to 1:30 p.m. and the afternoon values from 2 p.m. to 5:30 p.m.

Variable (unit) / r^2 (RMSE)	Daily	Morning	Midday	Afternoon
GPP ($\mu\mathrm{mol\,m^{-2}\,s^{-1}}$)	0.80 (1.99)	0.75 (2.65)	0.78 (2.62)	0.69 (2.23)
Red region SIF ($\mathrm{Wm^{-2}s^{-1}nm^{-1}sr^{-1}}$)				
mSCOPE	0.67 (0.29)	0.59 (0.37)	0.68 (0.36)	0.63 (0.24)
L2SM	0.62 (0.30)	0.59 (0.38)	0.62 (0.34)	0.60 (0.26)
LZ	0.63 (0.67)	0.59 (0.80)	0.65 (0.78)	0.58 (0.59)
Far-red region SIF ($\mathrm{Wm^{-2}s^{-1}nm^{-1}sr^{-1}}$)				
mSCOPE	0.74 (0.28)	0.74 (0.35)	0.76 (0.36)	0.70 (0.25)
L2SM	0.70 (0.37)	0.73 (0.45)	0.69 (0.42)	0.66 (0.33)
LZ	0.73 (1.37)	0.73 (1.61)	0.73 (1.67)	0.66 (1.23)

Table S3. The r^2 and RMSE values of simulated versus observed red and far-red region SIF values, according to different radiative transfer approaches at FI-Sod. The metrics are also shown for GPP, which is from default QUINCY configuration. The morning values are from 6 a.m. to 9:30 a.m., midday values from 10 a.m. to 1:30 p.m. and the afternoon values from 2 p.m. to 5:30 p.m.

Variable (unit) / r^2 (RMSE)	Daily	Morning	Midday	Afternoon
GPP ($\mu\mathrm{mol\,m^{-2}\,s^{-1}}$)	0.90 (0.87)	0.91 (0.99)	0.91 (1.08)	0.91 (1.07)
Red region SIF ($\mathrm{Wm^{-2}s^{-1}nm^{-1}sr^{-1}}$)				
mSCOPE	0.88 (0.13)	0.86 (0.14)	0.81 (0.26)	0.65 (0.16)
L2SM	0.85 (0.33)	0.86 (0.36)	0.81 (0.36)	0.58 (0.35)
LZ	0.82 (0.87)	0.84 (0.95)	0.80 (0.93)	0.57 (0.86)
Far-red region SIF ($\mathrm{Wm^{-2}s^{-1}nm^{-1}sr^{-1}}$)				
mSCOPE	0.87 (0.20)	0.86 (0.22)	0.79 (0.25)	0.65 (0.21)
L2SM	0.88 (0.36)	0.88 (0.40)	0.82 (0.40)	0.59 (0.36)
LZ	0.87 (1.33)	0.87 (1.40)	0.84 (1.47)	0.59 (1.32)

Table S4. Absolute values for different radiative transfer approaches and observations at the three sites, and overestimation of simulations compared to observations is in parenthesis calculated for July-August midday values (10 a.m. to 1:30 p.m) at the three sites. Overestimation is calculated by dividing the simulated value by the observed value, it thus shows how many times the simulation is overestimating the measured value.

Values (Overestimation) ($\mathrm{Wm^{-2}s^{-1}nm^{-1}sr^{-1}}$)	CA-Obs	US-NR1	FI-Sod
Red region SIF			
Observation	0.15 (-)	0.13 (-)	0.23 (-)
mSCOPE	0.63 (4.15)	0.60 (4.53)	0.43 (1.94)
L2SM	0.66 (4.37)	0.56 (4.28)	0.55 (2.46)
LZ	1.21 (7.98)	1.15 (8.62)	1.10 (4.94)
Far-red region SIF			
Observation	0.36 (-)	0.36 (-)	0.18 (-)
mSCOPE	0.79 (2.22)	0.82 (2.27)	0.36 (2.84)
L2SM	0.96 (2.70)	0.87 (2.46)	0.51 (4.04)
LZ	2.75 (7.67)	2.59 (7.20)	1.54 (12.32)

Table S5. Parameter values with their uncertainties in parenthesis from fit to hyperbolic function ($y = ax/(b+x)$), shown in Figure 6. The r^2 and the RMSE (units $\mu mol\, m^{-2}\, s^{-1}$)values are given additionally.

Set of points	a	b	r^2	RMSE
Observations				
CA-Obs	22.26 (0.70)	0.25 (0.02)	0.54	3.07
US-NR1	15.80 (0.70)	0.19 (0.02)	0.45	2.98
FI-Sod	11.47 (0.37)	0.05 (0.01)	0.35	1.89
Simulations				
CA-Obs	21.62 (0.32)	0.61 (0.02)	0.84	1.56
US-NR1	17.97 (0.57)	0.45 (0.04)	0.66	2.44
FI-Sod	13.87 (0.42)	0.39 (0.03)	0.69	1.01

Table S6. The metrics (r^2, RMSE and bias) of the simulated SIF at CA-Obs and FI-Sod against the TROPOSIF observations. The simulated values have been calculated from the midday values and TROPOSIF values are daily averages. The values are separately region around the site expanding to 0.50° x 0.50° or 0.25° x 0.25°. The units of RMSE and bias are $\mathrm{W m^{-2} s^{-1} nm^{-1} sr^{-1}}$.

Site and region	r^2	RMSE	Bias
CA-Obs (0.50° x 0.50°)	0.48	0.58	0.46
CA-Obs (0.25° x 0.25°)	0.46	0.65	0.56
FI-Sod (0.50° x 0.50°)	0.15	0.63	0.52
FI-Sod (0.25° x 0.25°)	0.26	0.66	0.59

S3 Supplementary figures

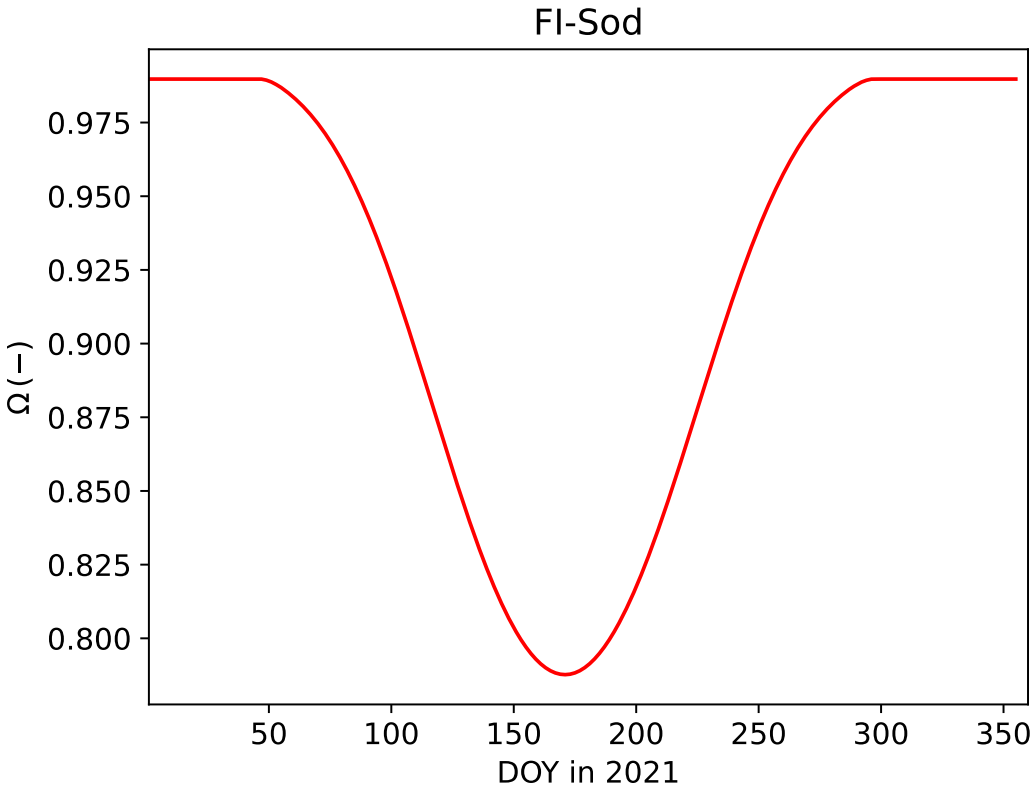

Figure S1. Midday (10 am - 1:30 pm) averages of the clumping index (Ω) by QUINCY model for the FI-Sod site in year 2021.

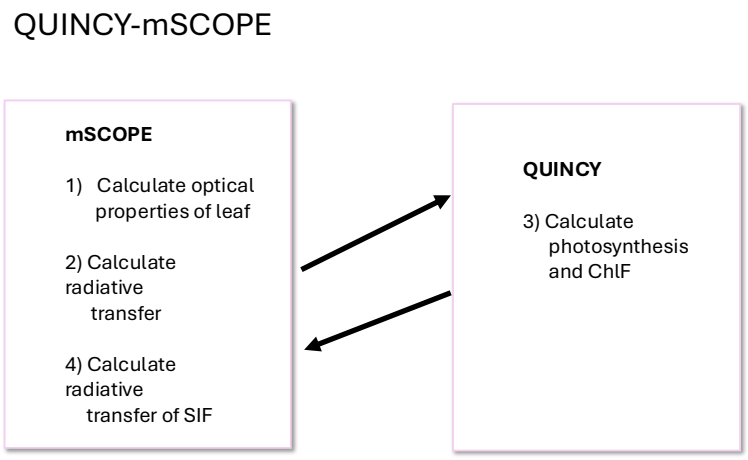

Figure S2. Conceptual figure of mSCOPE implementation in QUINCY. ChlF denotes chlorophyll fluorescence.

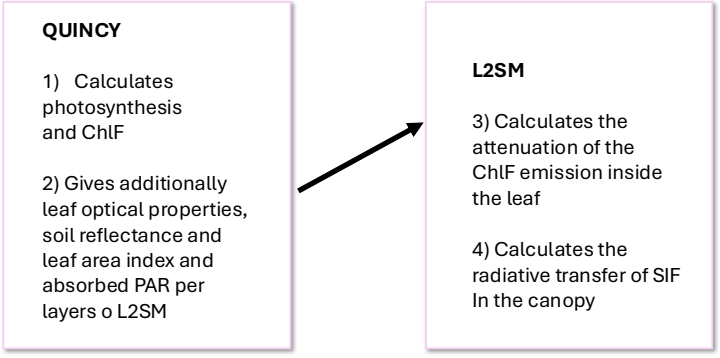

Figure S3. Conceptual figure of QUINCY and L2SM. ChlF denotes chlorophyll fluorescence and PAR is the photosynthetically active radiation.

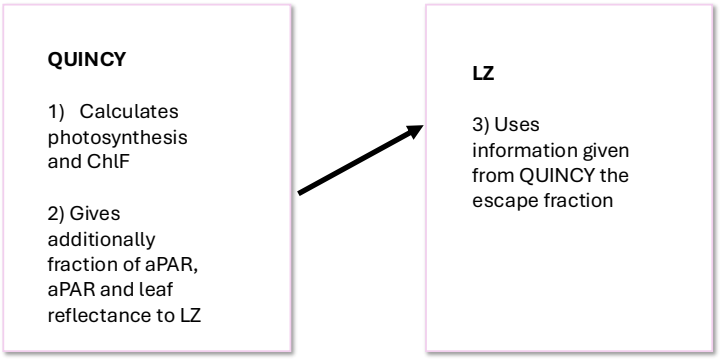

Figure S4. Conceptual figure of QUINCY and LZ. ChlF denotes chlorophyll fluorescence and PAR is the photosynthetically active radiation.

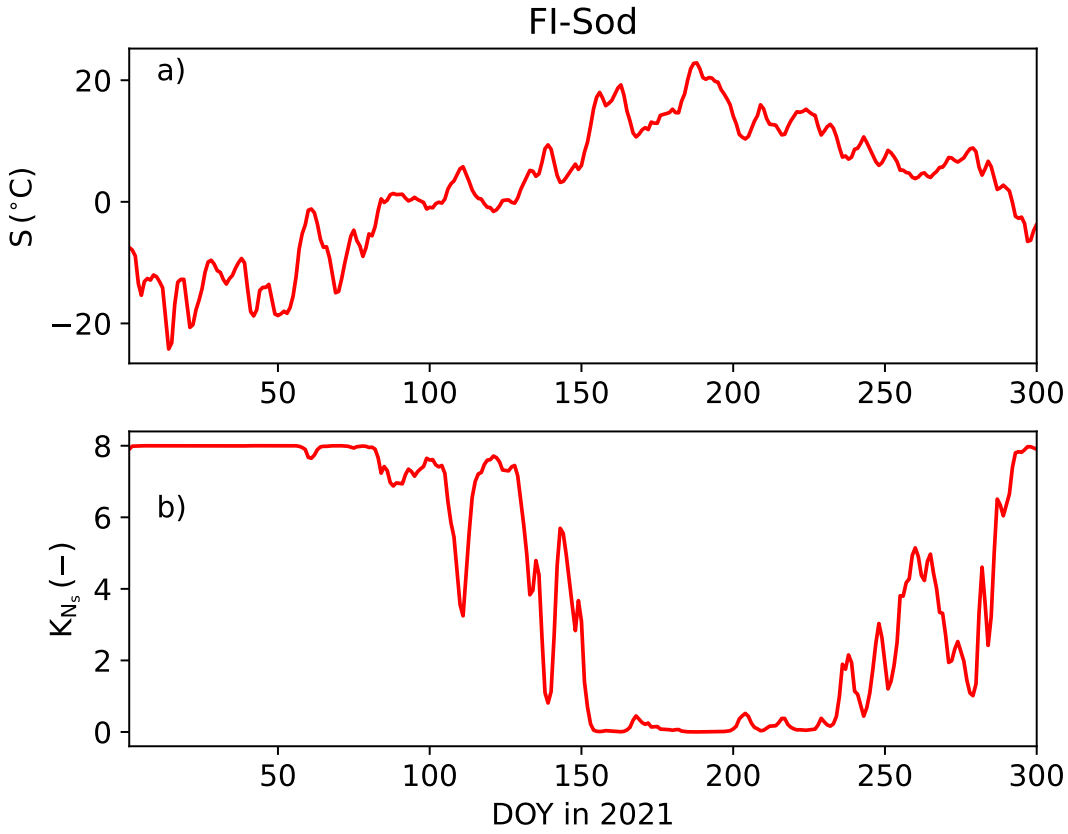

Figure S5. Seasonal cycle (DOY 1-300) of (a) the state of acclimation (S) and (b) K_{N_s} at FI-Sod in 2021.

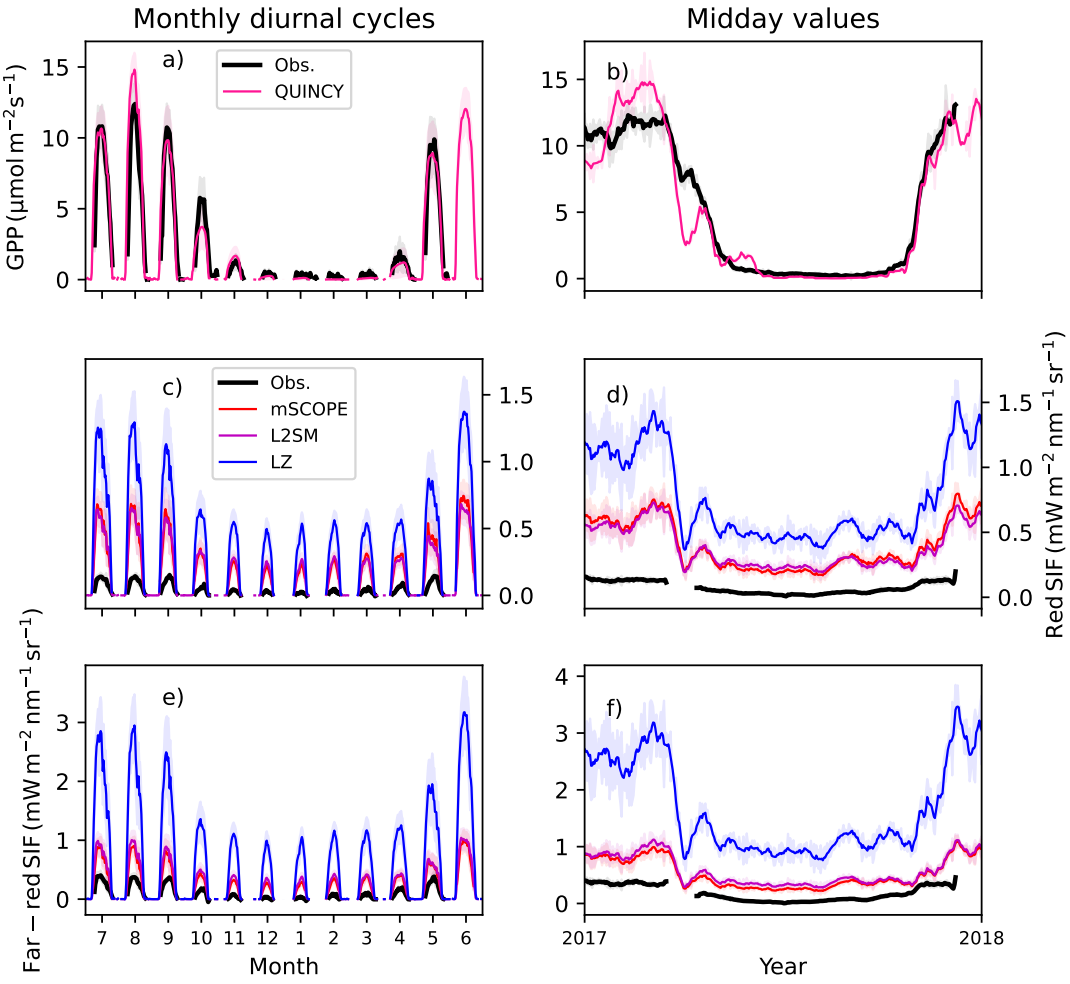

Figure S6. The monthly diurnal cycles for (a) GPP, (c) red region SIF and (e) far-red SIF and midday values, calculated from winter time between 10 a.m. and 1:30 p.m., for (b) GPP, (d) red region SIF, and (f) far-red SIF at US-NR1. The black line is in all plots observation, the pink line in the GPP plots is the QUINCY simulation results. For the SIF plots, red line is the mSCOPE results, magenta the L2SM and blue the LZ approach.

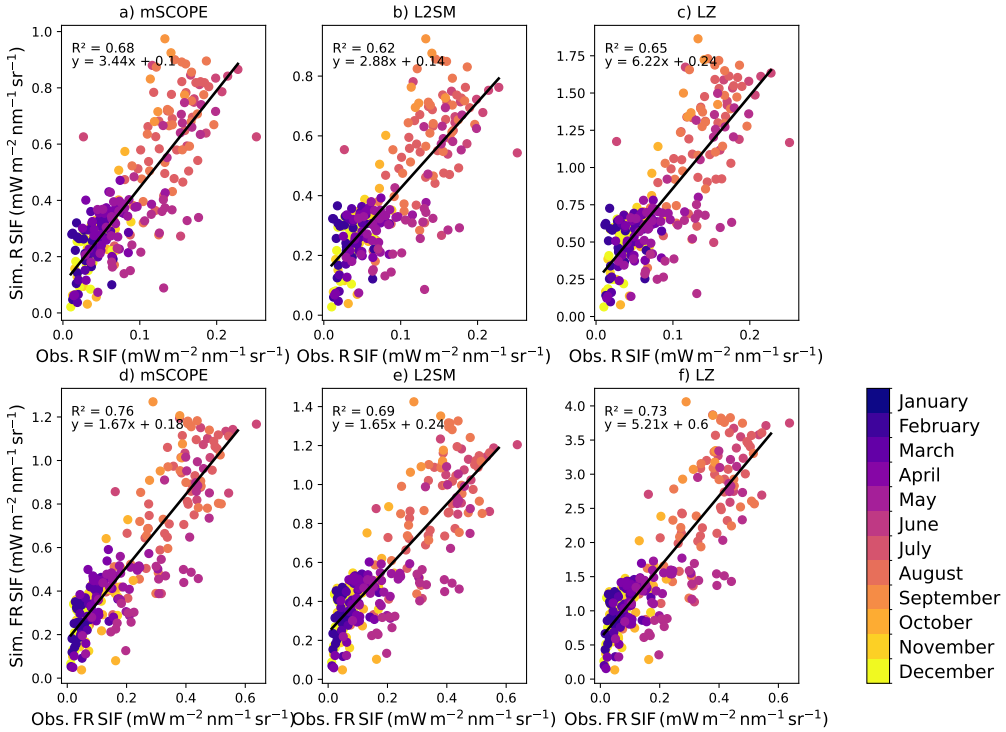

Figure S7. Observed vs. modelled SIF midday values in red (denoted with R in the figure) region (a: mSCOPE, b: L2SM, c: LZ) and far-red (denoted with FR in the figure) region (d: mSCOPE, e: L2SM: f: LZ) at US-NR1. Values from different months are color-coded. The black line show a fit with corresponding parameters shown in each panel. Months from June to December are from year 2017 and months January to May from 2018.

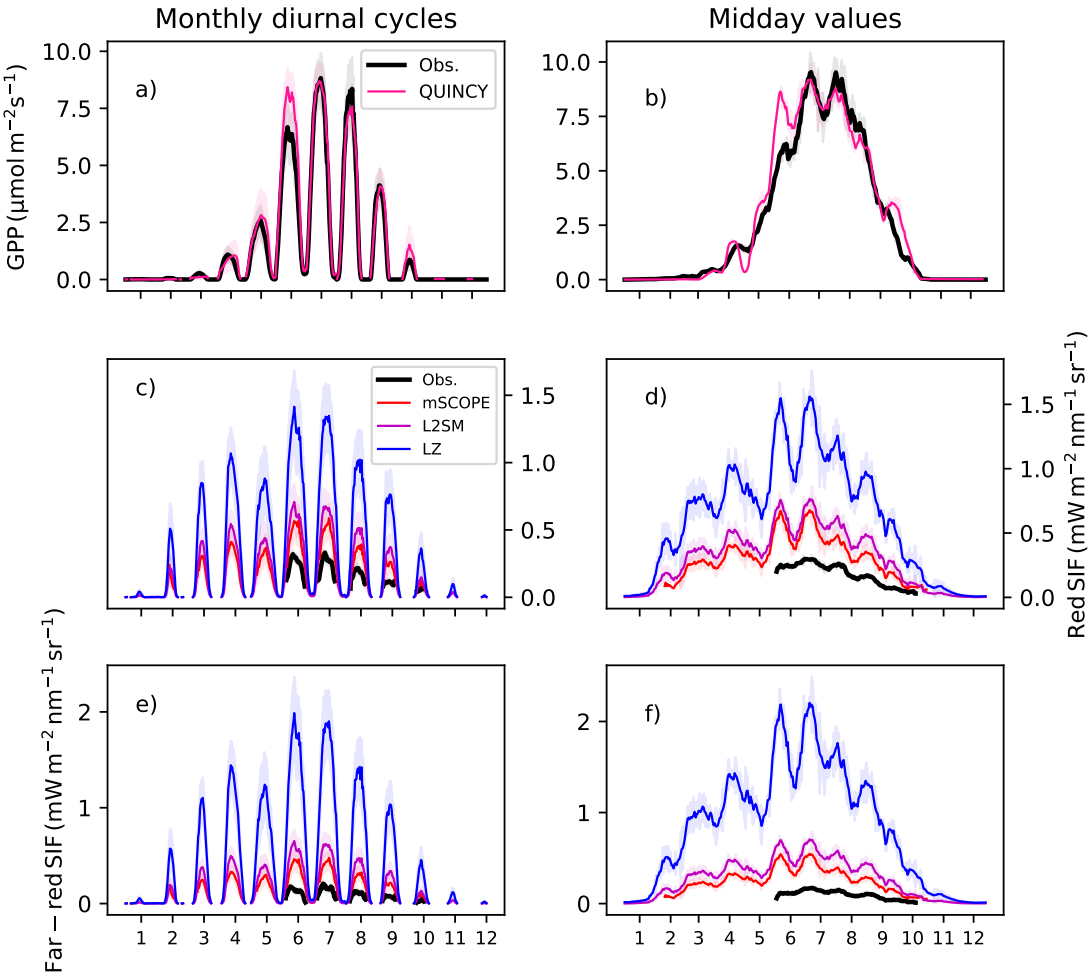

Figure S8. The monthly diurnal cycles for (a) GPP, (c) red region SIF and (e) far-red SIF and midday values, calculated from winter time between 10 a.m. and 1:30 p.m., for (b) GPP, (d) red region SIF, and (f) far-red SIF at FI-Sod. The black line is in all plots observation, the pink line in the GPP plots is the QUINCY simulation results. For the SIF plots, red line is the mSCOPE results, magenta the L2SM and blue the LZ approach.

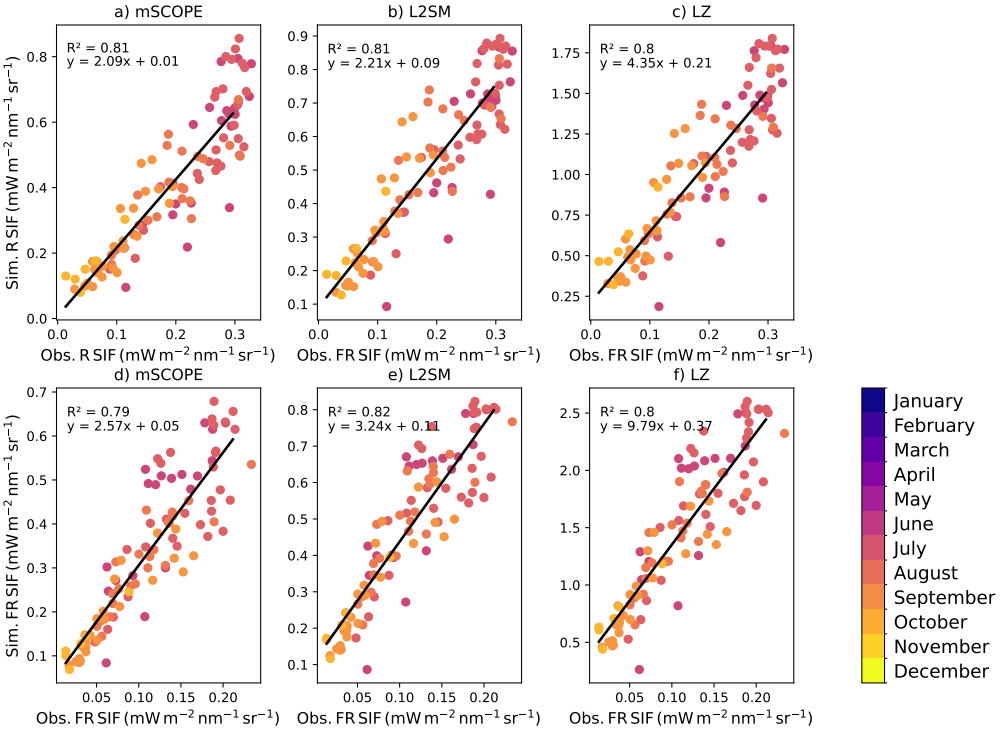

Figure S9. Observed vs. modelled SIF midday values in red (denoted with R in the figure) region (a: mSCOPE, b: L2SM, c: LZ) and far-red (denoted with FR in the figure) region (d: mSCOPE, e: L2SM: f: LZ) at FI-Sod. Values from different months are color-coded. The black line show a fit with corresponding parameters shown in each panel.

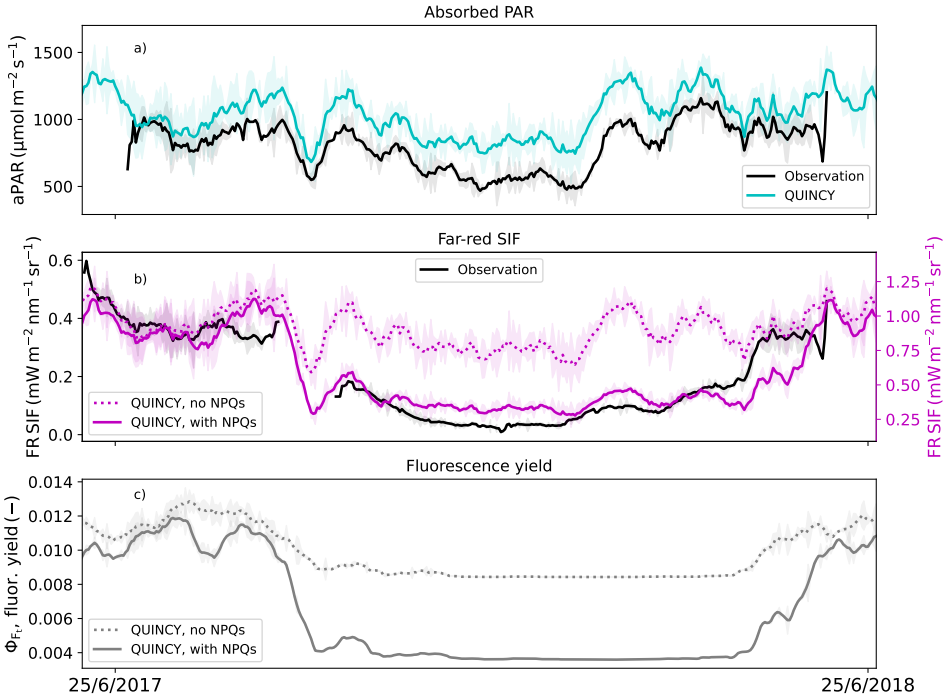

Figure S10. (a) The observed and simulated absorbed radiation at US-NR1, (b) far red (FR) region SIF values with and without sustained NPQ simulated with L2SM and (c) simulated chlorophyll fluorescence yields with and without sustained NPQ. The simulations have been done using L2SM. The values are averages of midday (10 a.m. to 2 p.m.) values, the standard deviation is shown as shaded regions.

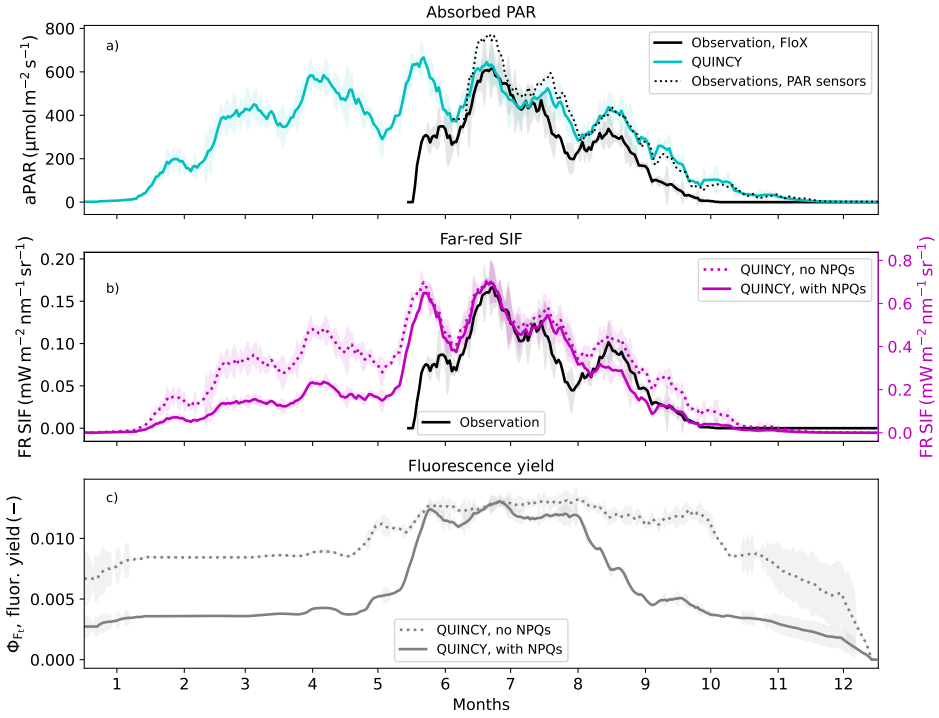

Figure S11. (a) The observed and simulated absorbed radiation at FI-Sod, (b) far red (FR) region SIF values with and without sustained NPQ simulated with L2SM and (c) simulated chlorophyll fluorescence yields with and without sustained NPQ. The simulations have been done using L2SM. The values are averages of midday (10 a.m. to 2 p.m.) values, the standard deviation is shown as shaded regions.

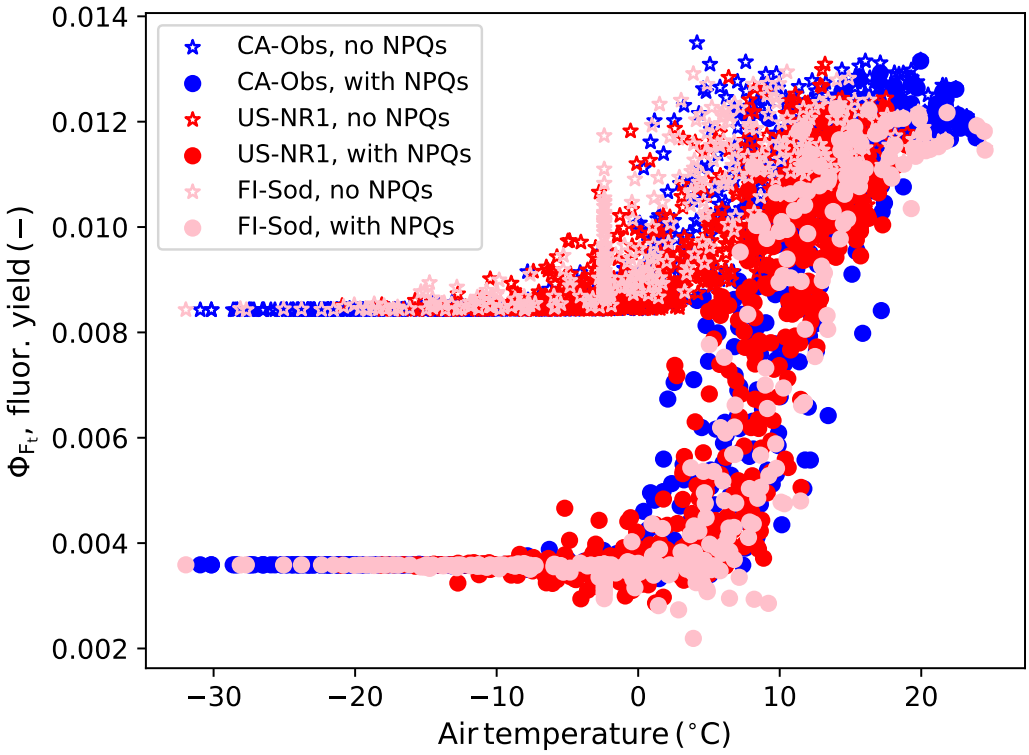

Figure S12. Temperature response of simulated chlorophyll fluorescence yield (Φ_F) when the $\mathrm{NPQ_s}$ was included in the calculation or not. The values are daily averages and the Φ_F is for the upmost canopy layer.

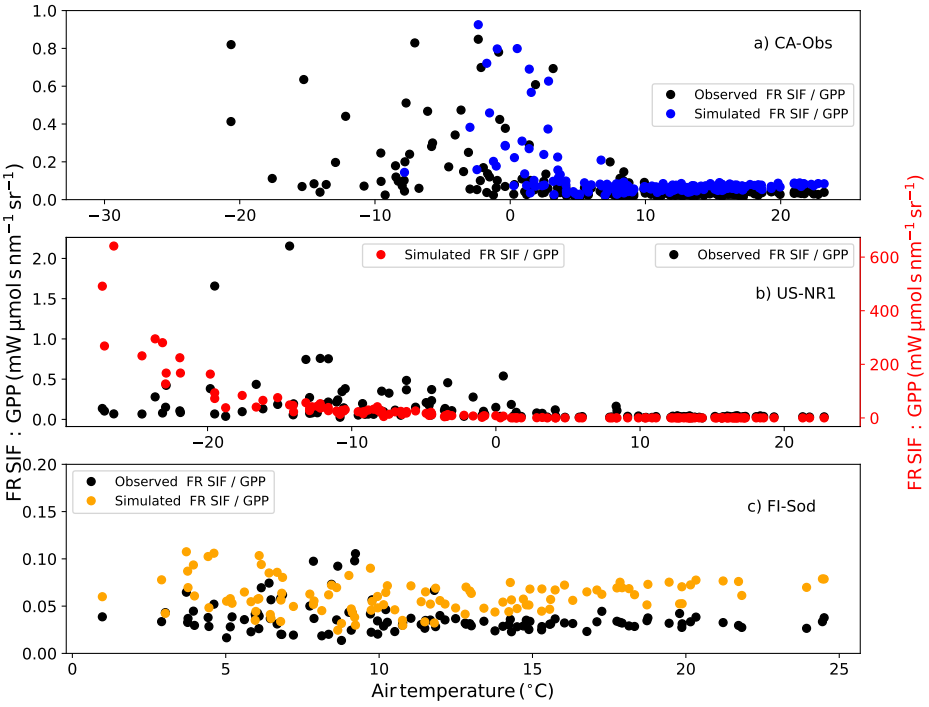

Figure S13. Temperature response of observed and simulated far-red SIF / GPP at (a) CA-Obs, (b) US-NR1 and (c) FI-Sod. The ratios have been calculated from the daily values. In (a) the scale on the y-axis has been set to be between zero and and one to make the variation around zero degrees visible. Part of the simulated values are therefore not displayed. In (b) the scale on the y-axis has been set to display the whole range of variation (the simulations have a distinct y-axis, while the other subplots have the same y-axis for simulations and observations). In (c) the observations covered shorter time scale and did not cover large temperature range. Black dots show the observations and the colored points the simulations.

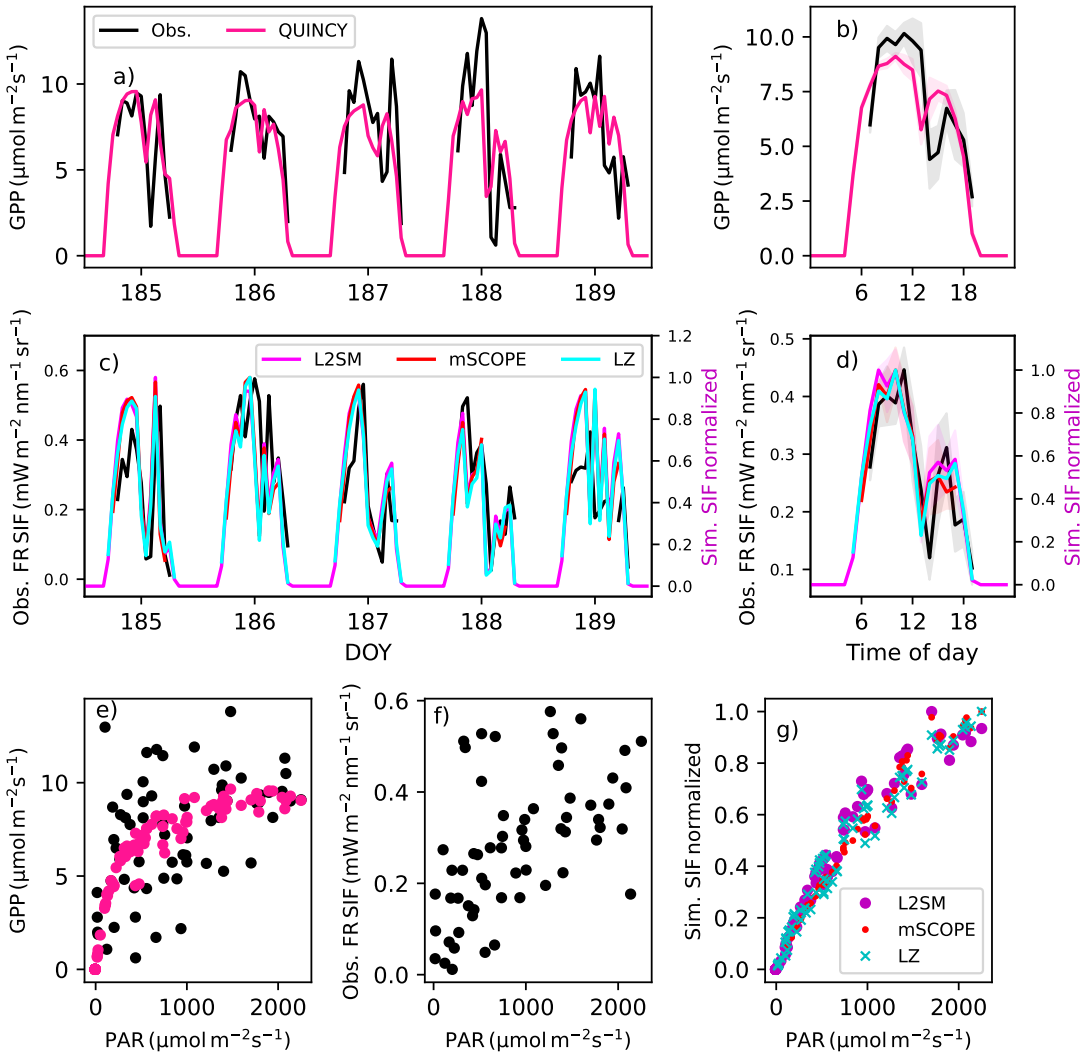

Figure S14. (a) The observed and simulated GPP and (c) far-red (denoted as FR in the figure) region SIF for days 185-189 (July 4-July 8, 2017) and averaged over these five days (b for GPP and d for far-red region SIF) at US-NR1. The shaded regions in b and d show the standard deviations of the averaged values. (e) The light response of the observed and simulated GPP for these five days, (f) the observed far-red region SIF and the (g) simulated far-red region SIF. The observations are in black, simulated GPP in pink and simulated far-red region SIF in magenta or L2SM, red for mSCOPE and cyan for the LZ approach.

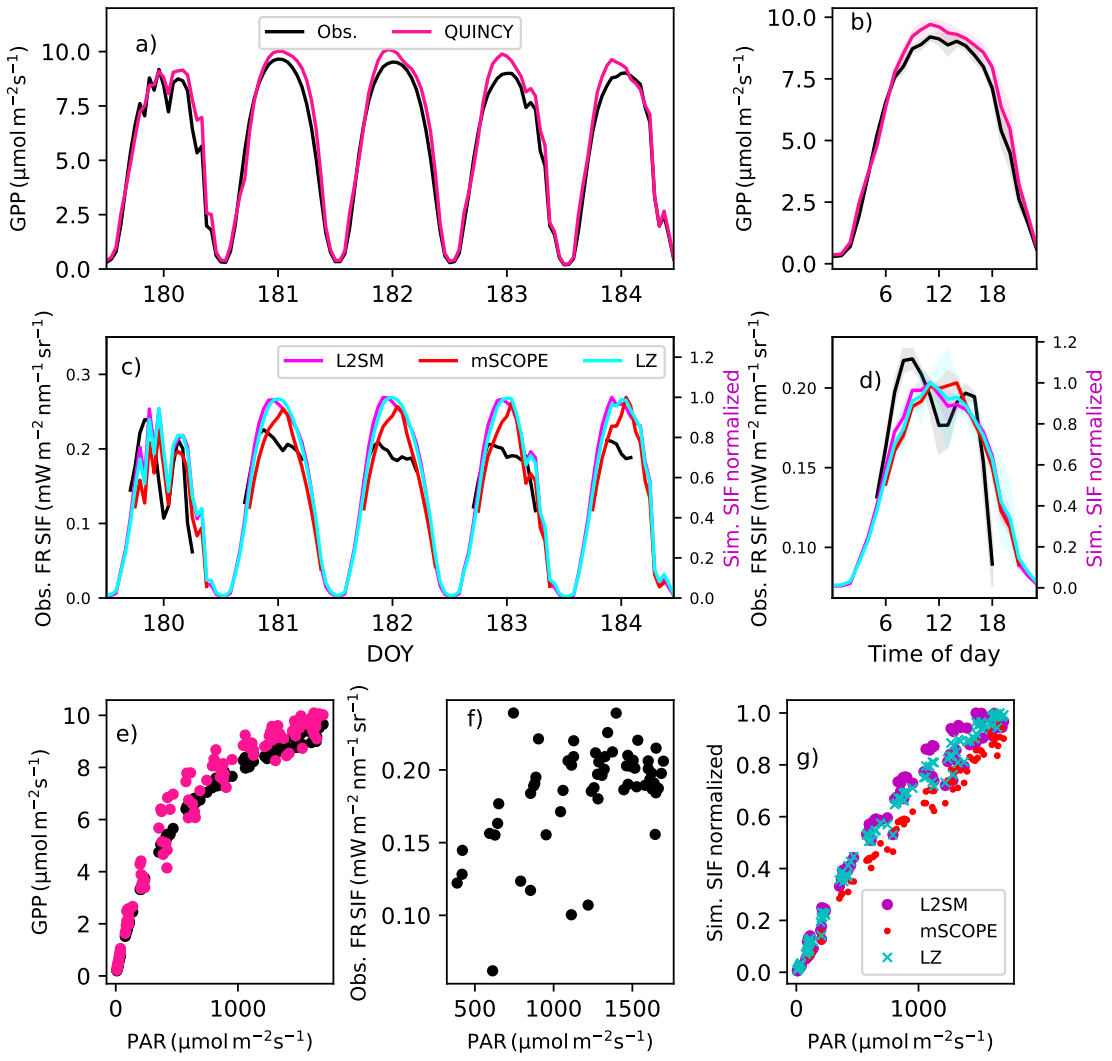

Figure S15. (a) The observed and simulated GPP and (c) far-red (denoted as FR in the figure) region SIF for days 180-184 (June 29-July 3, 2021) and averaged over these five days (b for GPP and d for far-red region SIF) at US-FI-Sod. The shaded regions in b and d show the standard deviations of the averaged values. (e) The light response of the observed and simulated GPP for these five days, (f) the observed far-red region SIF and the (g) simulated far-red region SIF. The observations are in black, simulated GPP in pink and simulated far-red region SIF in magenta for L2SM, red for mSCOPE and cyan for the Zeng approach.

References

Baldocchi, D., Falge, E., Gu, L., Olson, R., Hollinger, D., Running, S., Anthoni, P., Bernhofer, C., Davis, K., Evans, R., Fuentes, J., Goldstein, A., Katul, G., Law, B., Lee, X., Malhi, Y., Meyers, T., Munger, W., Oechel, W., Paw, K. T., Pilegaard, K., Schmid, H. P., Valentini, R., Verma, S., Vesala, T., Wilson, K., and Wofsy, S.: FLUXNET: A New Tool to Study the Temporal and Spatial Variability of Ecosys-

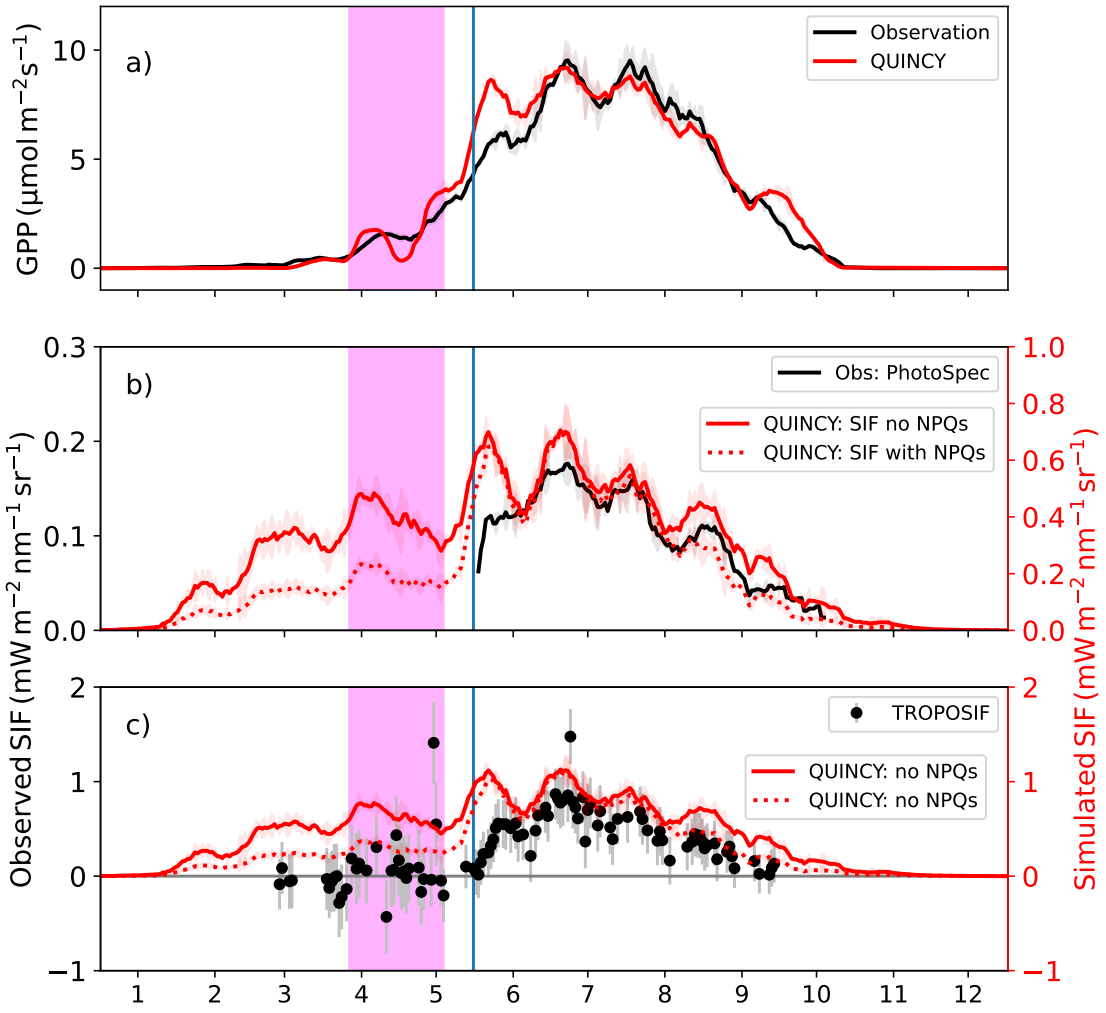

Figure S16. (a) The observed and simulated GPP at FI-Sod, (b) far-red region SIF from FloX observations and simulations with L2SM and (c) TROPOSIF observations and simulations with L2SM at 740 nm. The other values than TROPOSIF are averages of midday (10 a.m. to 1:30 p.m.) values, with standard deviation is shown as shaded areas and TROPOSIF uncertainty shown in error bars (c). TROPOSIF values are averages of the observations that took place that day. All the lines for midday values have been smoothed with a 15-day long window. Shaded region is from April 9th to May 17th, and the vertical like May 29th.

tem–Scale Carbon Dioxide, Water Vapor, and Energy Flux Densities, Bulletin of the American Meteorological Society, 82, 2415–2434, https://doi.org/10.1175/1520-0477(2001)082<2415:FANTTS>2.3.CO;2, 2001.

Evans, J. R.: Photosynthesis and nitrogen relationships in leaves of C3 plants, Oecologia, 78, 9–19, 1989.

Friend, A., Stevens, A., Knox, R., and Cannell, M.: A process-based, terrestrial biosphere model of ecosystem dynamics (Hybrid v3.0), Ecological Modelling, 95, 249–287, https://doi.org/10.1016/S0304-3800(96)00034-8, 1997.

Friend, A. D.: Modelling canopy CO2 fluxes: are 'big-leaf'simplifications justified?, Global ecology and biogeography: a journal of macroecology, 10, 603–619, https://nph.onlinelibrary.wiley.com/doi/abs/10.1046/j.1466-822x.2001.00268.x, 2001.

Genty, B., Briantais, J.-M., and Baker, N. R.: The relationship between the quantum yield of photosynthetic electron transport and quenching of chlorophyll fluorescence, Biochimica et Biophysica Acta (BBA) - General Subjects, 990, 87–92, https://doi.org/https://doi.org/10.1016/S0304-4165(89)80016-9, 1989.

Gordon, H. R.: Diffuse reflectance of the ocean: The theory of its augmentation by chlorophyll a fluorescence at 685 nm, Applied Optics, 18, 1161–1166, https://doi.org/10.1364/AO.18.001161, 1979.

Kattge, J., Díaz, S., Lavorel, S., Prentice, I. C., Leadley, P., Bönisch, G., Garnier, E., Westoby, M., Reich, P. B., Wright, I. J., Cornelissen, J. H. C., Violle, C., Harrison, S. P., Van Bodegom, P. M., Reichstein, M., Enquist, B. J., Soudzilovskaia, N. A., Ackerly, D. D., Anand, M., Atkin, O., Bahn, M., Baker, T. R., Baldocchi, D., Bekker, R., Blanco, C. C., Blonder, B., Bond, W. J., Bradstock, R., Bunker, D. E., Casanoves, F., Caverner-Bares, J., Chambers, J. Q., Chapin III, F. S., Chave, J., Coomes, D., Cornwell, W. K., Craine, J. M., Dobrin, B. H., Duarte, L., Durka, W., Elser, J., Esser, G., Estiarte, M., Fagan, W. F., Fand, J., Fernández-Méndez, F., Fidelis, A., Finegan, B., Flores, O., Ford, H., Frank, D., Freschet, G. T., Fyllas, N. M., Gallagher, R. V., Green, W. A., Gutierrez, A. G., Thomas, H., Higgins, S. I., Hodgson, J. G., Jalili, A., Jansen, S., Joly, C. A., Kerkhoff, A. J., Kirkup, D., Kitajima, K., Kleyer, M., Klotz, S., Knops, J. M. H., Kramer, K., Kühn, I., Kurokawa, H., Laughlin, D., Lee, T. D., Leishman, M., Lens, F., Lenz, T., Lewis, S. L., Lloyd, J., Llusià, J., Louault, F., Ma, S., Mahecha, M. D., Manning, P., Massad, T., Medlyn, B. E., Messier, J., Moles, A. T., Müller, S. C., Nadrowski, K., Naeem, S., Niinemets, Ü., Nöllert, S., Nüske, A., Ogaya, R., Oleksyn, J., Onipchenko, V. G., Onoda, Y., Ordoñez, J., Overbeck, G., Ozinga, W. A., Patino, S., Paula, S., Pausas, J. G., Peñuelas, J., Phillips, O. L., Pillar, V., Poorter, H., Poorter, L., Poschlod, P., Prinzing, A., Proulx, R., Rammig, A., Reinsch, S., Reu, B., Sack, L., Salgado-Negret, B., Sardans, J., Shiodera, S., Shipley, B., Siefert, A., Sosinski, E., Soussana, J. F., Swaine, E., Swenson, N., Thompson, K., Thornton, P., Waldram, M., Weiher, E., White, M., White, S., Wright, S. J., Yguel, B., Zaehle, S., Zanne, A. E., and Wirth, C.: TRY - a global database of plant traits, Global Change Biology, 17, 2905–2935, 2011.

Knorr, W., Williams, M., Thum, T., Kaminski, T., Voßbeck, M., Scholze, M., Quaife, T., Smallman, T. L., Steele-Dunne, S. C., Vreugdenhil, M., Green, T., Zaehle, S., Aurela, M., Bouvet, A., Bueechi, E., Dorigo, W., El-Madany, T. S., Migliavacca, M., Honkanen, M., Kerr, Y. H., Kontu, A., Lemmetyinen, J., Lindqvist, H., Mialon, A., Miinalainen, T., Pique, G., Ojasalo, A., Quegan, S., Rayner, P. J., Reyes-Muñoz, P., Rodríguez-Fernández, N., Schwank, M., Verrelst, J., Zhu, S., Schüttemeyer, D., and Drusch, M.: A comprehensive land-surface vegetation model for multi-stream data assimilation, D&B v1.0, Geoscientific Model Development, 18, 2137–2159, https://doi.org/10.5194/gmd-18-2137-2025, 2025.

Magney, T. and Frankenberg, C.: Chlorophyll fluorescence spectra for a wide range of species and conditions, https://doi.org/10.22002/D1.1226, funding by NASA, 2019.

Magney, T. S., Bowling, D. R., Logan, B. A., Grossmann, K., Stutz, J., Blanken, P. D., Burns, S. P., Cheng, R., Garcia, M. A., Köhler, P., Lopez, S., Parazoo, N. C., Raczka, B., Schimel, D., and Frankenberg, C.: Mechanistic evidence for tracking the seasonality of photosynthesis with solar-induced fluorescence, Proceedings of the National Academy of Sciences, 116, 11 640–11 645, https://doi.org/10.1073/pnas.1900278116, 2019.

Mäkelä, J., Knauer, J., Aurela, M., Black, A., Heimann, M., Kobayashi, H., Lohila, A., Mammarella, I., Margolis, H., Markkanen, T., Susiluoto, J., Thum, T., Viskari, T., Zaehle, S., and Aalto, T.: Parameter calibration and stomatal conductance formulation comparison for boreal forests with adaptive population importance sampler in the land surface model JSBACH, Geoscientific Model Development, 12, 4075–4098, https://doi.org/10.5194/gmd-12-4075-2019, 2019.

Medlyn, B. E., Duursma, R. A., Eamus, D., Ellsworth, D. S., Prentice, I. C., Barton, C. V. M., Crous, K. Y., De Angelis, P., Freeman, M., and Wingate, L.: Reconciling the optimal and empirical approaches to modelling stomatal conductance, Global Change Biology, 17, 2134–2144, https://doi.org/https://doi.org/10.1111/j.1365-2486.2010.02375.x, 2011.

Mäkelä, A., Hari, P., Berninger, F., Hänninen, H., and Nikinmaa, E.: Acclimation of photosynthetic capacity in Scots pine to the annual cycle of temperature, Tree Physiology, 24, 369–376, https://doi.org/10.1093/treephys/24.4.369, 2004.

Niinemets, Ü., Kull, O., and Tenhunen, J. D.: An analysis of light effects on foliar morphology, physiology, and light interception in temperate deciduous woody species of contrasting shade tolerance, Tree Physiology, 18, 681–696, https://doi.org/10.1093/treephys/18.10.681, 1998.

Thum, T., Aalto, T., Laurila, T., Aurela, M., Lindroth, A., and Vesala, T.: Assessing seasonality of biochemical CO_2 exchange model parameters from micrometeorological flux observations at boreal coniferous forest, Biogeosciences, 5, 1625–1639, https://doi.org/10.5194/bg-5-1625-2008, 2008.

Thum, T., Caldararu, S., Engel, J., Kern, M., Pallandt, M., Schnur, R., Yu, L., and Zaehle, S.: A new model of the coupled carbon, nitrogen, and phosphorus cycles in the terrestrial biosphere (QUINCY v1.0; revision 1996), Geoscientific Model Development, 12, 4781–4802, https://doi.org/10.5194/gmd-12-4781-2019, 2019.

van der Tol, C., Verhoef, W., Timmermans, J., Verhoef, A., and Su, Z.: An integrated model of soil-canopy spectral radiances, photosynthesis, fluorescence, temperature and energy balance, Biogeosciences, 6, 3109–3129, https://doi.org/10.5194/bg-6-3109-2009, 2009.

van der Tol, C., Berry, J. A., Campbell, P. K. E., and Rascher, U.: Models of fluorescence and photosynthesis for interpreting measurements of solar-induced chlorophyll fluorescence, Journal of Geophysical Research: Biogeosciences, 119, 2312–2327, https://doi.org/10.1002/2014JG002713, 2014.

Willmott, C. J.: On the validation of models, Physical Geography, 2, 184–194, https://doi.org/10.1080/02723646.1981.10642213, 1981.

Yang, P., Verhoef, W., and van der Tol, C.: The mSCOPE model: A simple adaptation to the SCOPE model to describe reflectance, fluorescence and photosynthesis of vertically heterogeneous canopies, Remote Sensing of Environment, 201, 1–11, https://doi.org/https://doi.org/10.1016/j.rse.2017.08.029, 2017.

Zaehle, S. and Friend, A.: Carbon and nitrogen cycle dynamics in the O-CN land surface model: 1. Model description, site-scale evaluation, and sensitivity to parameter estimates, Global Biogeochemical Cycles, 24, 2010.